

## A LOW NOISE TRIPLE PHASE SLEEP SIGNAL SLEW RATE MODULATION USED IN MTCMOS CIRCUITS

<sup>1</sup>P. Bala Krishna, <sup>2</sup>A. Ravindar, <sup>3</sup>Priyanka Saxena

<sup>1,2,3</sup>Electronics and Communication Engineering, Keshav Memorial Institute of Technology, Narayanaguda, Hyderabad

**Abstract**--Triple phase Sleep signal slew rate modulation techniques for suppressing mode-transition noise are explored in this paper. A triple-phase sleep signal slew rate modulation (TPS) technique with a novel digital sleep signal generator is proposed. Reactivation time, mode-transition energy consumption, leakage power consumption, and layout area of different MTCMOS circuits are characterized under an equal-noise constraint. Influences of within-die and die-to-die parameter variations on the reactivation noise, time, and energy consumption of sleep signal slew rate modulated MTCMOS circuits are evaluated with a process imperfections aware robustness metric. The proposed triple-phase sleep signal slew rate modulation technique enhances the tolerance to process parameter fluctuations by up to  $183.1\times$  as compared to various alternative MTCMOS noise suppression techniques in a UMC 80-nm CMOS technology.

**Keywords**--low noise, mode transition energy, power and ground bouncing noise, process variations, reactivation time, sleep signal rise delay, triple-phase wake-up.

### I. Introduction

MULTI-THRESHOLD CMOS (MTCMOS), also known as power/ground gating, is the most commonly used circuit technique for leakage power reduction. An integrated circuit is typically divided into multiple autonomous power/ground gating domains for effective reduction of leakage power consumption. When an idle circuit is awoken, high currents flow through the sleep transistors. Significant voltage fluctuations occur on the power and ground distribution networks (power and ground bouncing noise). Mode transition noise produced by an awakening circuit block propagates to the already active circuit blocks in the neighboring domains through the shared power and ground distribution networks. Logic states of internal nodes in surrounding active circuits are disturbed due to significant noise. Increasing numbers of (finer-grain) independently power/ground-gated logic and memory domains are employed for enhanced energy efficiency in modern integrated circuits. With more frequent transitions between the ACTIVE and SLEEP modes of operation to achieve more effective leakage power savings; reactivation noise has become an important reliability concern in modern integrated circuits. Sleep signal slew rate modulation techniques are presented in this paper for suppressing the power and ground distribution network noise that are produced by MTCMOS circuits. Multi-phase sleep signal slew rate modulation techniques are investigated to mitigate noise while significantly reducing reactivation time and energy consumption in MTCMOS circuits. The reactivation time, mode transition energy consumption, leakage power consumption, and layout area of MTCMOS circuit techniques are characterized under an equal noise constraint. The impact of process variations on the reactivation noise, time, and energy consumption of

MTCMOS circuits is also evaluated. This paper is organized as follows. An alternative triple-phase sleep signal slew rate modulation (TPS) technique is presented in Section II. A new fully digital triple-phase sleep signal generator is proposed. The previously published stepwise V<sub>gs</sub> MTCMOS circuit technique is reviewed in Section III. Different design options are presented in Section IV to modulate the slew rate of activation signals in MTCMOS circuits under an equal-noise constraint.

### II. Triple-Phase Sleep Signal Slew Rate Modulation

A slowly rising sleep signal is ineffective for suppressing the reactivation noise in MTCMOS circuits. A slowly rising sleep signal, however, also significantly increases the reactivation time and energy consumption of MTCMOS circuits. The single-phase sleep signal slew rate modulation technique is therefore not suitable for fast and energy efficient power/ground gating in high-performance integrated circuits. An alternative triple-phase sleep signal slew rate modulation (TPS) technique is presented in to suppress the reactivation noise while accelerating the reactivation process in MTCMOS circuits. The concept of TPS. As discussed in Section II, the sleep transistor produces negligible noise in the weak inversion region of operation (when  $V_{gs} < V_{th\text{sleep}}$ ). The sleep signal is preferred to rise faster from 0 V to the threshold voltage of sleep transistor in order to reduce the overall reactivation time without producing significant noise. Reactivation noise is primarily produced after the sleep transistor is turned on. The sleep signal should be therefore subsequently decelerated as the gate voltage level reaches the threshold voltage of sleep transistor. Deceleration of sleep signal suppresses the peak mode transition noise that is produced after the sleep transistor is fully activated. After the VGND voltage is reduced to a very low

level close to 0 V (time point  $t_B$  as shown in Fig. 4), the mode transition noise diminishes to a negligibly low level. The rise of sleep signal should therefore be again accelerated to shorten the remaining duration of reactivation process. Due to the shorter periods of Phase\_1 and Phase\_3, the reactivation time and energy consumption of MTCMOS circuits are reduced with the TPS technique as compared with the single-phase sleep signal slew rate modulation technique that is presented in Section II.A. A mixed-signal switched capacitor circuit is proposed for triple-phase sleep signal slew rate modulation in. The mixed-signal sleep signal modulator is shown in Fig. 1. The  $V_{gs}$  of sleep transistor is increased with small voltage steps. Additional clock signal and voltage bias sources ( $V_{bias1}$ ,  $V_{bias2}$ , and  $V_{bias3}$ ) are required for the operation of this mixed-signal circuit. Complex analog circuitry is employed to produce the three phases of sleep transistor activation. The mixed-signal sleep signal modulator consumes significant power and occupies a large layout area. The rising speed of sleep signal cannot be tuned individually during Phase\_1 and Phase\_2 with the sleep signal modulator that is described in Phase\_1 is inevitably elongated together with Phase\_2 to suppress the reactivation noise. The triple-phase reactivation time reduction that is achievable with this mixed-signal sleep signal generator is therefore limited. Furthermore, the sleep signal slew rates during Phase\_1 and Phase\_2 strongly depend on the value of  $C_{pump}$  [see Fig. 1(a)]. Variations of  $C_{pump}$  due to process fluctuations significantly degrade the effectiveness of this mixed-signal modulator for noise suppression. A digital circuit is presented in for triple-phase sleep signal slew rate modulation. The sleep signal modulator is effective for reducing the reactivation noise, time, and energy consumption of MTCMOS circuits as compared to the single-phase sleep signal slew rate modulation technique. The deactivation process (ACTIVE to SLEEP mode transition) with this digital sleep signal modulator is, however, overlooked in. During a deactivation event, high short-circuit currents are produced by the digital sleep signal modulator, thereby causing a significant amount of energy consumption. A new superior fully digital triple-phase sleep signal slew rate modulator is proposed in this paper. The circuit is shown in Fig. 6. Sleep Global is the input signal of the new sleep signal modulator. Sleep Global triggers the activation and deactivation procedures of an MTCMOS circuit block. Sleep Local is produced by the proposed signal modulator and applied to the gate terminal of the sleep transistor that controls the ground connection of a local circuit. P1, P2, and P3 are used for tuning the slew rate of Sleep Local during reactivation events that occur in three phases. The new triple-phase sleep signal slew rate modulator operates as follows. In SLEEP mode, Sleep Global is "0." P1, P2, and P3 are cut off. Ndischarge is turned on. Sleep Local is maintained at  $\sim 0$  V. The sleep transistor is cut off. EN1 is maintained

at  $V_{DD}$  by Preset1 that is turned on in SLEEP mode. Sleep Global transitions from "0" to  $V_{DD}$  to initiate a reactivation event. PH1 transitions to low. P1 is turned on to start the first phase (Phase\_1) of reactivation. Sleep Local starts to rise. When Sleep Local reaches the threshold voltage of  $N_{senseL}$  (low- $|V_{th}|$ ),  $N_{senseL}$  is turned on. EN1 is discharged through  $N_{reset1}$  and  $N_{senseL}$ . PH1 transitions to high. P1 is cut off. PH2 transitions to low. P2 is thereby turned on to start the second phase (Phase\_2) of reactivation, where the sleep signal slew

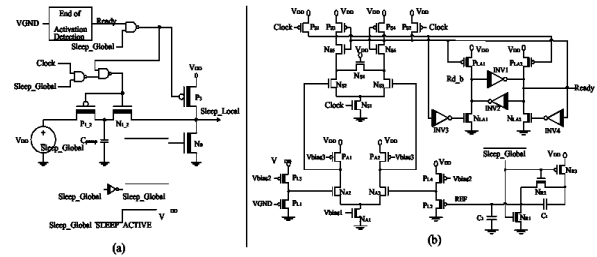


Fig.1. Schematic of the previously published mixed-signal triple-phase sleep signal slew rate modulator (TPS old). "Virtualground line of the ground-gated MTCMOS circuit. High- $|V_{th}|$  transistors and CMOS logic gates are represented with thick lines in the transistor and gates symbols, respectively. (a) Circuit structure of TPS old. (b) Schematic of the "end of activation detection" circuit block.

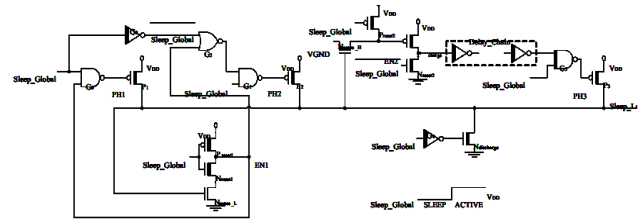


Fig.2. Schematic of the new fully digital triple-phase sleep signal slew rate modulator. "Sleep Global" is the input signal coming from the on-chip power management unit. Rate is reduced. The VGND is discharged primarily during Phase\_2. Highest switching currents are produced in this phase as the internal nodes in the awakening low- $|V_{th}|$  circuit block transition to correct logic states. The rise of Sleep Local is intentionally decelerated by turning on P2 while cutting off P1 in Phase\_2. P2 is designed (sized) to be significantly weaker as compared to P1. The peak reactivation noise produced by an awakening MTCMOS circuit is thereby mitigated. When the VGND is discharged to a relatively low voltage level, the voltage difference between Sleep Local and VGND becomes higher than the threshold voltage of  $N_{senseH}$  (high- $|V_{th}|$ ).  $N_{senseH}$  is turned on. EN2 (maintained at  $V_{DD}$  in SLEEP mode) is discharged. Pcharge is activated. After the delay of "Delay Chain" and G5, PH3 transitions to low. P3 is turned on to start the third phase (Phase\_3) of reactivation where the rate of

change of Sleep Local is increased again. Weak P2 is maintained on to assist the significantly stronger P3 as Sleep Local is raised faster toward VDD in Phase\_3. During a deactivation event, Sleep Global transitions from VDD to "0." PH1, PH2, and PH3 transition to high after the delay of G0, G1 and G5, respectively. P1, P2, and P3 are cut off. Alternatively Ndischarge is turned on after the delay of G4. Sleep Local is discharged to ~0V by Ndischarge, thereby deactivating the MTCMOS circuit. Since P1, P2, and P3 are disabled before Ndischarge is turned on, no short-circuit current is produced by P1, P2, and P3 in this new digital sleep signal modulator.

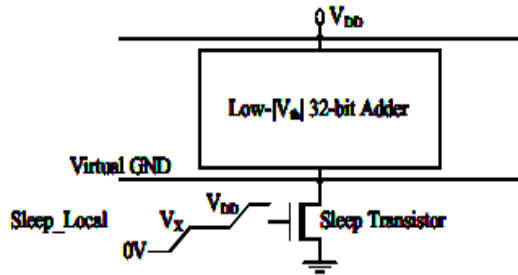


Fig.3. Illustration of the stepwise Vgs MTCMOS circuit technique. High-|Vth| sleep transistor is represented with a thick line in the channel area.

With the triple-phase sleep signal slew rate modulator that is shown in Fig. 6, the rising speed of sleep signal is adjusted by monitoring the voltage level of Sleep Local and VGND. The transitions between the three phases of reactivation occur automatically. No additional control signals or voltage bias sources are required by the new sleep signal slew rate modulator. Furthermore, the proposed sleep signal modulator is a digital circuit with lower power consumption, smaller area, and enhanced immunity to process variations as compared to the mixed-signal sleep signal modulator circuit that is presented in. Although the triple-phase sleep signal slew rate modulation idea is discussed in, the effectiveness of the TPS technique for suppressing mode transition noise and reducing reactivation delay is not quantitatively evaluated in Three implementations of the TPS technique with the previously published mixed-signal sleep signal slew rate modulator, the digital sleep signal modulator that is presented in, and the new digital sleep signal modulator that is shown in Fig. 6 are characterized in the following sections of this paper.

### III. Step Wise Vgs MTCMOS

The previously published [7] stepwise Vgs MTCMOS circuit technique to suppress mode transition noise is reviewed in this section. The stepwise Vgs MTCMOS circuit technique is illustrated in Fig. 7. The slew rate modulation technique is also applied to the stepwise Vgs MTCMOS circuit in this paper. The slew

rate modulated stepwise Vgs MTCMOS circuit is evaluated in the subsequent sections. A stepwise Vgs MTCMOS circuit is activated in two steps as follows. The sleep signal transitions from 0 V to an intermediate voltage level VX (0 V < VX < VDD) during the first step of a reactivation event. The sleep transistor is weakly activated with a low gate voltage (VX). Although the voltage swing on the VGND is relatively high during the first wake up step, the amplitude of the first noise waveform is suppressed due to the weak conductivity of the sleep transistor. After the VGND is discharged to a sufficiently low voltage level, the sleep signal transitions from VX to VDD. The sleep transistor is strongly turned on. VGND is discharged to ~0 V following the full activation of the sleep transistor (Sleep\_Local = VDD). The amplitude of the second noise waveform is also suppressed due to the lower voltage swing on the VGND during the second wake up step.

A Sleep signal modulator for stepwise Vgs MTCMOS circuit is presented in [8]. The circuit is shown in Fig. 8. During the

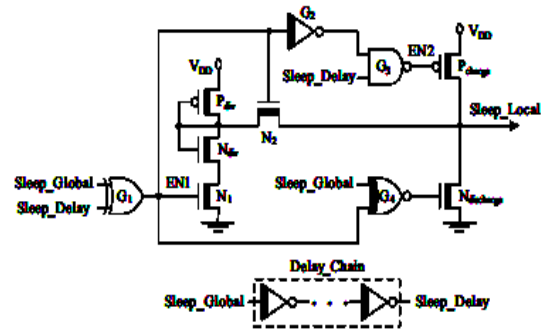


Fig.4. Schematic of the sleep signal modulator for stepwise Vgs MTCMOS circuit. "Sleep Global" is the input signal coming from the on-chip power management unit.

"Sleep Local" is the sleep signal applied to the local ground-gated MTCMOS circuit block. High-|Vth| transistors and CMOS logic gates are represented with thick lines in the transistor and gate symbols, respectively.

First wake up step, N2 is turned on. Pdiv and N2 raise Sleep\_Local from 0 V to VX. The value of VX is determined by the voltage divider that is composed of the diode-connected pMOS transistor Pdiv, diode-connected nMOS transistor Ndiv, and N1. During the second wake up step, N2 is cut off, while Pcharge is activated. Sleep\_Local is raised from VX to VDD by Pcharge. While the stepwise Vgs is a potentially effective technique for mode transition noise suppression, many practical design challenges of stepwise Vgs MTCMOS circuits are over-looked in. The methodology needed to choose an appropriate intermediate voltage VX is not provided. The influence of sleep signal slew rate on reactivation noise is not discussed. The

optimum  $V_X$  that minimizes the peak reactivation noise varies with the threshold voltage of sleep transistor. The effectiveness of stepwise  $V_{gs}$  in suppressing reactivation noise is therefore strongly affected by process variations. Parameter fluctuations and other implementation challenges of stepwise  $V_{gs}$  MTCMOS circuits are discussed in detail in the following sections of this paper.

**IV. Sleep Signal Slew Rate Modulation Techniques Under Equal-Noise Constraint**

Single-phase sleep signal slew rate modulation, triple-phase sleep signal slew rate modulation, and stepwise  $V_{gs}$  MTCMOS circuit techniques are evaluated in this section under an equal noise constraint. The sleep signal waveforms are tuned to suppress the peak ground bouncing noise to a negligible level that is less than 2 mV with different MTCMOS circuit techniques. Peak noise voltages that are less than 2 mV are considered to be negligibly small in this paper. The reactivation delay and energy consumption of MTCMOS circuits are evaluated with this noise criterion. The Reactivation Delay is  $Reactivation\ Delay = \text{Max}\{Ground\ Stability\ Delay, Sleep\ Local\ Delay\}$  (1) where Ground Stability Delay is the time interval from Sleep Local rises to 10 mV until the virtual ground voltage

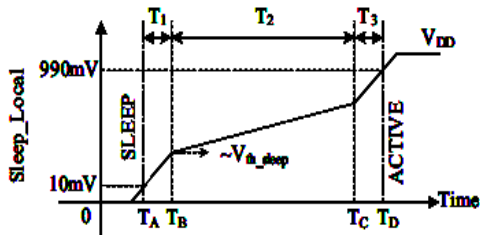


Fig.5. Timing diagram of the local sleep signal with the TPS MTCMOS circuit.

Stabilizes below 10mV. Sleep\_Local\_Delay is the time interval from Sleep\_Local rises to 10 mV until Sleep\_Local stabilizes above 990 mV.

**A. Single-Phase Sleep Signal Slew Rate Modulation**

The design of single-phase sleep signal slew rate modulated MTCMOS circuit is briefly described in this section. In order to satisfy the maximum acceptable ground bouncing noise criterion of 2 mV, the rise delay of single-phase sleep signal (Sleep\_Local\_Delay) needs to be at least 43.40 ns.

The sleep signal slew rate modulator for the single-phase sleep signal slew rate modulated MTCMOS circuit is composed of two inverters. The rise delay of the single-phase sleep signal is modulated by tuning the size of the pull-up transistor (Psingle\_charge) in the second-stage inverter of the sleep signal slew rate modulator.

**B. Triple-Phase Sleep Signal Slew Rate Modulation**

The design of TPS MTCMOS circuit to satisfy the equal noise constraint is presented in this section. The timing diagram of the local sleep signal with the TPS MTCMOS circuit is illustrated in Fig. 9. At TA, Sleep\_Local reaches 10mV. PH2 is discharged to VDD/2 (halfway through the high-to-low transition voltage swing) and P2 is effectively turned on at TB. The delay of the feedback loop (composed of Nreset1, Nsense\_L, and G0 in Fig. 6) is tuned to ensure that P1 is cut off by the time Sleep\_Local rises to the threshold voltage of sleep transistor ( $V_{Sleep\_Local} \sim V_{th\_sleep} \sim 370\text{ mV}$  [23]). Duration of Phase\_1 (T1) is the time interval from TA to TB. By adjusting the delay of the feedback loop composed of Nsense\_H, Pcharge, "Delay\_Chain" (in Fig. 6), and G5, P3 is activated after the VGND is discharged to 10 mV. PH3 is discharged to VDD/2 (halfway through the high-to-low transition voltage swing) and P3 is effectively turned on at TC. Duration of Phase\_2 (T2) is the time interval from TB to TC. At TD, Sleep\_Local rises to 990 mV. Duration of Phase\_3 (T3) is the time interval from TC to TD.

The values of T1 and T2 are tuned to suppress the peak ground bouncing noise to a negligible level below 2 mV. Furthermore, T1 is modulated to minimize the energy delay product (EDP) during the first two phases of reactivation. The EDP is

$$EDP = \text{Phase}_{1+2}\ Energy \times \text{Phase}_{1+2}\ Delay \quad (2)$$

Where Phase<sub>1+2</sub> Delay is the duration of Phase\_1 and Phase\_2 (T1 + T2). Phase<sub>1+2</sub> Energy is the total energy consumed by

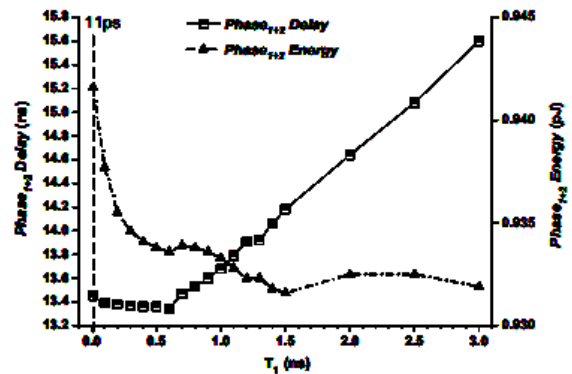


Fig.6. Phase<sub>1+2</sub> Delay and Phase<sub>1+2</sub> Energy of TPS MTCMOS circuit for different durations of Phase\_1. T1 is varied from 11 ps to 3 ns. 11 ps is approximately the minimum achievable 10 to 370 mV rise delay in this UMC 80-nm CMOS technology.

The MTCMOS circuit during Phase\_1 and Phase\_2. When T1 is relatively small ( $T1 < 600\text{ ps}$ ), the noise produced during Phase\_1 affects the subsequent Phase\_2 noise. For these relatively short durations of Phase\_1 ( $T1 < 600\text{ ps}$ ), decreasing T1 requires an increase in T2 to be

able to satisfy the maximum acceptable noise criterion of 2 mV. The overall Phase1+2 Delay is thereby increased with reduced T1 for T1 < 600ps as shown in Fig. 10. Alternatively, when T1 is relatively large (T1 > 600ps), the influence of noise produced during Phase\_1 is small on Phase\_2 noise. The duration of Phase\_2 that is required to satisfy the equal-noise constraint is therefore maintained approximately constant (T2 variation less than 1.5%) for 600 ps < T1 < 3 ns. Phase1+2 Delay is increased approximately linearly with T1 for T1 > 600 ps as shown in Fig. 10. The minimum Phase1+2 Delay is observed when T1 is 600 ps. The voltage swings of the VGND and the internal nodes of low-|Vth| 32-bit adder are similar during T1 and T2. When T1 is increased, the variation of Phase1+2 Energy is therefore negligible (less than 1.06% variation as T1 is increased from

11ps to 3 ns) as shown in Fig. 10. Similar to the minimum Phase1+2 Delay, the minimum EDP is also observed when T1 is 600ps as shown in Fig. 11. For this optimum duration of Phase\_1 (T1 = 600 ps), T2 needs to be at least 12.75 ns to satisfy the peak acceptable ground bouncing noise criterion of 2 mV. At the end of Phase\_2, the sleep signal rises to 636 mV and the VGND is discharged to 10 mV.

The reactivation noise is primarily produced during Phase\_2. The duration of Phase\_3 (T3) has no significant influence on the peak ground bouncing noise. T3, however, affects the energy consumption and delay of a reactivation event. Duration of Phase\_3 (T3) is therefore important and tuned to lower the Reactivation EDP (REDP). The REDP is

$$REDP = Wake\_Up\_Energy \times Reactivation\_Delay \quad (3)$$

Where Wake\_Up\_Energy is the total energy consumed by the MTCMOS circuit during the period of Reactivation\_Delay. The Reactivation\_Delay is defined in (1). The Reactivation\_Delay and Wake\_Up\_Energy of the MTCMOS circuit are monotonically increased with a longer T3 as shown in Fig. 12. The REDP therefore monotonically increases with longer

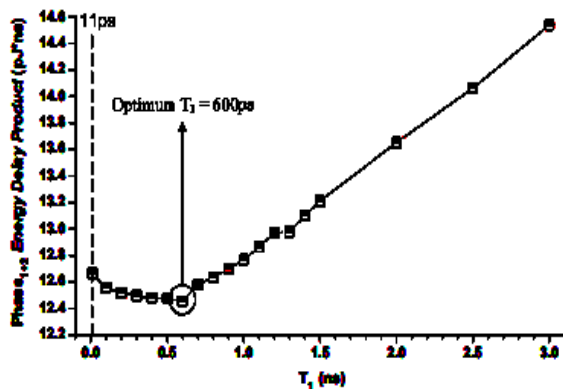


Fig.7. EDP of the first two phases of reactivation with the TPS MTCMOS circuit. T1 is varied from 11ps to 3 ns.

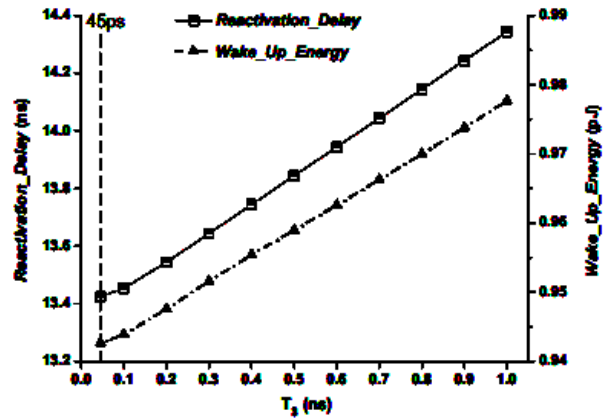


Fig.8. Reactivation Delay and Wake up Energy of TPS MTCMOS circuit for different durations of Phase\_3. T3 is varied from 45ps to 1ns. 45ps is approximately the minimum achievable 636 to 990 mV rise delay in this UMC 80-nm CMOS technology.

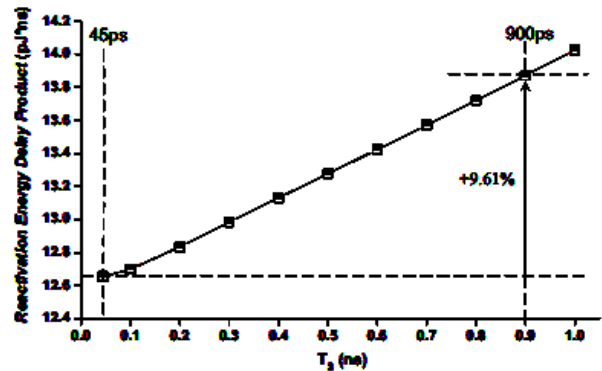


Fig.9. RED P of TPS MTCMOS circuit for different durations of Phase\_3. T3 is varied from 45ps to 1ns.

T3 as shown in Fig.13. Minimum REDP is observed with T3=45 ps. To be able to realize the design option that requires the shortest possible Phase\_3 duration of 45ps, P3 (in the triple phase sleep signal slew rate modulator that is shown in Fig. 6) has to be a very wide low-|Vth| transistor (width of P3 is

Table I  
Parameters For Achieving Equal Noise With Sleep Signal Slew Rate Modulation Techniques

Circuit technique	Critical parameters
Single-phase	Rise delay of sleep signal: 43,40 ns.
TPS	T1: 600 ps; T2: 12.75 ns; T3: 900 ps.
Stepwise Vgs	Vχ: 0.49 V; TR_first: 1.9 ns; TR_second: 1.1 ns; Trelax: 10.76 ns.

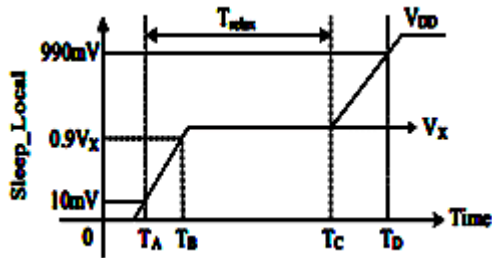


Fig.10. Timing diagram of the local sleep signal with the step wise Vgs MTCMOS circuit.

14.5 $\mu$ m) [6]. High instantaneous currents are produced by the large P3 when Phase\_3 is initiated during a wake-up event. Significant amount of additional switching noise is therefore produced and injected onto the ground distribution network by the triple-phase sleep signal modulator. The equal noise constraint is actually violated when the sleep signal modulator noise is included in the analysis ( $T3 = 45$  ps) [6]. Due to the high noise produced by the sleep signal slew rate modulator, the power and ground distribution networks are further disturbed, thereby delaying the reactivation of TPS MTCMOS circuit as well [see the definition of Reactivation\_Delay in (1)]. Furthermore, higher leakage power and layout area overhead are caused by the sleep signal modulator when P3 is sized large enough to minimize  $T3$  [6]. In order to avoid the high overhead of the design option with  $T3 = 45$  ps, an alternative TPS MTCMOS circuit with a longer Phase\_3 ( $T3 = 900$  ps) is preferred in this paper. As shown in Fig. 13, when  $T3$  is increased from 45 to 900 ps, the REDP difference is less than 10%. The critical timing parameters of this preferred implementation of TPS are listed in Table I.

**C. Sleep Signal Slew Rate Modulated Stepwise Vgs MTCMOS Circuit**

The optimization of sleep signal slew rate modulated step wise Vgs MTCMOS circuit to satisfy the equal-noise constraint is presented in this section. The timing diagram of the local sleep signal with the stepwise Vgs MTCMOS circuit is illustrated in Fig. 14. The relaxation time ( $T_{relax}$ ) of stepwise Vgs MTCMOS circuit is the time interval from Sleep\_Local rises to 10 mV until the virtual ground voltage is discharged to the relaxation voltage ( $V_{relax}$ ).  $V_{relax}$  is

$$V_{relax} = \text{Max}\{1.1 * V_{stable}, 10 \text{ mV}\} \quad (4)$$

where  $V_{stable}$  is the steady state VGND voltage of the MTCMOS circuit when Sleep\_Local is  $V_X$ . At  $T_A$ , Sleep\_Local reaches 10 mV. At  $T_B$ , Sleep\_Local rises to  $0.9V_X$ . Sleep\_Local rise delay is the time interval from  $T_A$  to  $T_B$  during the first step of reactivation. The strength of

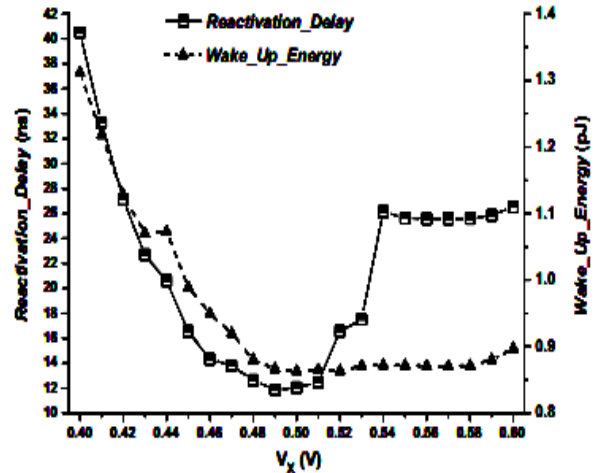


Fig.11. Reactivation\_Delay and Wake\_Up\_Energy of sleep signal slew rate modulated stepwise Vgs MTCMOS circuit for different  $V_X$ .

$P_{div}$  and  $N2$  (in Fig. 8) are tuned to ensure that Sleep\_Local rises to  $0.9V_X$  at  $T_B$ . By adjusting the delay of “Delay\_Chain,”  $G1$ ,  $G2$ , and  $G3$ , Pcharge is activated after the VGND is discharged to  $V_{relax}$ . EN2 is discharged to  $V_{DD}/2$  (halfway through the high-to-low transition voltage swing) and Pcharge is turned on at  $T_C$ .  $T_{relax}$  is the time interval from  $T_A$  to  $T_C$ . At  $T_D$ , Sleep\_Local rises to 990 mV. Sleep\_Local rise delay of the second step of reactivation is the time interval from  $T_C$  to  $T_D$ .

Sleep\_Local rise delays of the two phases of reactivation are tuned to suppress the peak ground bouncing noise below 2 mV with the stepwise Vgs MTCMOS circuit.  $V_X$  is optimized to minimize the REDP [defined in (3)]. For each value of  $V_X$ , Sleep\_Local rise delay (measured from 10 mV to  $0.9V_X$ ) of the first step of reactivation is increased from the minimum achievable rise delay until the first wave of ground bouncing noise is suppressed below 2 mV. Afterwards, Sleep\_Local rise delay (measured from  $V_X$  to 990 mV) of the second step of reactivation is increased from the minimum achievable rise delay until the second noise waveform is also suppressed below 2 mV. Variations of the Reactivation\_Delay [defined in (1)] and Wake\_Up\_Energy (defined in Section V-B) with  $V_X$  are shown in Fig. 15.

When  $V_X$  is relatively small (for example, 0.4 V), the VGND is discharged slowly by the weak sleep transistor during the first wake-up step. Furthermore, Sleep\_Local rise delay of the second step of reactivation needs to be increased to suppress the peak amplitude of the second noise wave form below 2 mV. The Reactivation\_Delay of stepwise Vgs MTCMOS circuit is thereby prolonged. Alternatively, when  $V_X$  is relatively large (for example, 0.6 V), Sleep\_Local rise delay of the

first step of reactivation needs to be elongated to suppress the peak amplitude of the first noise waveform below 2 mV. The reactivation time is thereby also increased with a relatively large VX in a stepwise Vgs MTCMOS circuit. The minimum Reactivation\_Delay is observed when VX is 0.49 V.

When VX is relatively small (for example, 0.4 V), the sleep transistor stays in the active region for a long time during the reactivation process. Significant leakage currents are produced by the low-|Vth| 32-bit adder. Furthermore, higher shortcircuit currents are produced during the reactivation process with small VX. Total Wake\_Up\_Energy of the stepwise Vgs MTCMOS circuit is thereby increased. As shown in Fig. 15, the Wake\_Up\_Energy of the stepwise Vgs MTCMOS circuit is significantly reduced (by 34.21%) when VX is increased from 0.4 to 0.5 V. The minimum Wake\_Up\_Energy is achieved when VX is 0.5 V. If VX is further increased beyond 0.5 V, the sleep transistor stays in the weak inversion region for a longer time during a reactivation event. The Wake\_Up\_Energy consumed due to leakage currents is thereby increased for VX > 0.5 V.

The REDP with different VX is shown in Fig. 16. Similar to the minimum Reactivation\_Delay, the minimum REDP of stepwise Vgs MTCMOS circuit is also observed when VX is 0.49 V. The critical voltage and timing parameters of the stepwise Vgs MTCMOS circuit technique are listed in Table I.

**V. Evaluation Of Sleep Signal Slew Rate Modulated Mtcmos Circuits**

Four different sleep signal modulators are designed to produce the real sleep signals for the ground-gated MTCMOS circuits according to the parameters that are listed in Table I. Both the digital sleep signal modulator (TPS\_A) that is presented in [6] and the new superior sleep signal modulator (TPS\_B) that is shown in Fig. 6 are characterized in this section. The sizes of critical transistors are listed in Table II. Channel lengths of some of the transistors are longer than 2λ for suppressing the short-channel effects and providing enhanced tolerance to process variations.

A fifth mixed-signal triple-phase sleep signal slew rate modulator (TPS\_old) is also designed and evaluated in this paper as shown in Fig. 5. The frequency of the clock signal that is required by TPS\_old (see Fig. 5) is assumed to be 1-GHz. Cpump is selected (Cpump is implemented with a metal-oxide-semiconductor capacitor in the UMC 80-nm CMOS technology: Cpump=0.5fF) to limit the peak noise to approximately 2 mV during Phase\_1 and Phase\_2 of reactivation. P3 is sized (see Table II) to guarantee that the peak noise produced during Phase\_3 is below 2 mV. The voltage at node “REF” [see Fig. 5(b)] is maintained at 10 mV. Phase\_3 is thereby initiated when

the VGND is

Table II  
Critical Transistor sizes in different MTCMOS Circuits

Circuit technique	Critical transistor sizes
Single-phase	$P_{single\ charge}: W = 120\text{ nm}/L = 2.06\ \mu\text{m}.$
TPS_old [10]	$P_{1,2}: W = 160\text{ nm}/L = 160\text{ nm}; N_{1,2}: W = 160\text{ nm}/L = 160\text{ nm}; P_3: W = 600\text{ nm}/L = 160\text{ nm}.$
TPS_A [6]	$P_1: W = 160\text{ nm}/L = 160\text{ nm}; P_2: W = 120\text{ nm}/L = 2.16\ \mu\text{m}; P_3: W = 780\text{ nm}/L = 160\text{ nm}.$
TPS_B (Fig. 6)	$P_1: W = 160\text{ nm}/L = 160\text{ nm}; P_2: W = 120\text{ nm}/L = 2.16\ \mu\text{m}; P_3: W = 780\text{ nm}/L = 160\text{ nm}.$
Stepwise Vgs (Fig. 8)	$P_{div}: W = 180\text{ nm}/L = 160\text{ nm}; N_{div}: W = 160\text{ nm}/L = 160\text{ nm}; P_{charge}: W = 420\text{ nm}/L = 160\text{ nm}; N_1: W = 160\text{ nm}/L = 160\text{ nm}; N_2: W = 240\text{ nm}/L = 160\text{ nm}.$

\*UMC 80-nm CMOS technology. Minimum channel width = 120 nm. Minimum channel length = 80 nm.

\*UMC 80-nm CMOS technology. Minimum channel width = 120 nm. Minimum channel length = 80 nm.

Discharged to ~10 mV during a reactivation event. As illustrated in Fig. 5, high-|Vth| transistors are extensively employed in the mixed-signal sleep signal modulator to minimize the leakage power consumption. The voltage bias sources (Vbias1 = 0.48 V, Vbias2 = 0.5 V, and Vbias3 = 0.5 V) that are utilized in the mixed-signal sleep signal modulator are assumed to be available on-chip. The leakage power and area overhead of the voltage bias generators are not considered in this paper.

With the sleep signal generators in place, design tradeoffs among overall reactivation time, overall reactivation energy consumption, overall deactivation energy consumption, leak-age power consumption, and layout areas of MTCMOS circuits are discussed in Section VI-A. The effects of process parameter variations on peak ground bouncing noise, overall reactivation time, and overall reactivation energy consumption of different MTCMOS circuits are evaluated in Section VI-B.

**A. Characterization of MTCMOS Circuits**

Various design metrics of MTCMOS circuits are characterized assuming the typical (nominal) process corner of UMC 80-nm CMOS technology in this section. The overall reactivation time (TR), overall reactivation energy (ER), overall deactivation energy (ED), SLEEP mode leakage power consumption, and layout areas of different sleep signal slew rate modulated MTCMOS circuits are listed in Table III. The overall reactivation time (TR) is

$$TR = \text{Sleep\_Signal\_Modulator\_Delay} + \text{Reactivation\_Delay}(5)$$

where the Sleep\_Signal\_Modulator\_Delay is the time interval from Sleep\_Global rises to 10 mV until Sleep\_Local rises to 10 mV. The Reactivation\_Delay is

defined in (1). The overall reactivation energy (ER) is the total energy consumed by a sleep signal modulator and MTCMOS circuit together during the overall reactivation time. The overall deactivation energy

(ED) is the total energy consumed by a sleep signal generator and MTCMOS circuit together during the deactivation delay (the time interval from Sleep\_Global falls to 10 mV until Sleep\_Local falls to 10 mV).

Various design metrics are compared among TPS\_A, TPS\_B, TPS\_old, stepwise Vgs, and single-phase sleep signal slew rate modulated MTCMOS circuits next. As listed in Table III, the stepwise Vgs MTCMOS circuit reduces the overall reactivation time by 72.46%, 43.46%, 16.09%, and 15.92% as compared to the single-phase, TPS\_old, TPS\_A, and TPS\_B MTCMOS circuits, respectively, when the five circuits are designed to produce similar ground bouncing noise. Due to the relatively shorter durations of Phase\_1 and Phase\_3, TPS\_B MTCMOS circuit reduces the overall reactivation time by 67.25% as compared to the single-phase MTCMOS circuit. The rising speed of sleep signal cannot be tuned individually during Phase\_1 and Phase\_2 with the mixed-signal triple-phase sleep signal slew rate modulator that is presented in [9]. Phase\_1 is therefore inevitably elongated together with Phase\_2 to suppress the reactivation noise, thereby increasing the overall reactivation time as compared to the TPS\_B MTCMOS circuit. TPS\_B MTCMOS circuit reduces the overall reactivation time by 32.76% as compared to the TPS\_old MTCMOS circuit.

The energy consumed during mode transitions is an important concern in MTCMOS circuits. Lower mode transition energy consumption enables an MTCMOS circuit to transition to SLEEP mode more frequently, thereby allowing more significant leakage power savings [16]-[19]. MTCMOS circuit techniques with suppressed mode transition energy consumption are therefore highly desirable. As listed in Table III, in addition to shortening the delay, TPS\_A, TPS\_B, and stepwise Vgs MTCMOS circuits also significantly lower the energy consumed during the reactivation events. Significant weak inversion currents are produced by the low-|Vth| 32-bit adder due to the longer reactivation process of the single phase MTCMOS circuit, thereby increasing the reactivation energy consumption by 1.93×, 1.92×, and 1.91× as compared to the stepwise Vgs, TPS\_A, and TPS\_B MTCMOS circuits, respectively. Due to the relatively longer reactivation time and the more complex and power hungry circuitry of the mixed-signal sleep signal modulator, the TPS\_old MTCMOS circuit consumes 53.67%, 52.48%, and 52.33% higher energy as compared to the stepwise Vgs, TPS\_A, and TPS\_B MTCMOS circuits, respectively, during reactivation events.

During the deactivation process with the stepwise

Vgs sleep signal modulator, Sleep\_Local transitions from ~ VDD to an intermediate voltage level (between VDD and 0 V) before being fully discharged to ~0 V. Significant short-circuit currents are produced by Pdiv, Ndiv, and N1. The stepwise Vgs MTCMOS circuit therefore increases the deactivation energy consumption by 15.59×, 7.91×, and 6.71× as compared to the single-phase, TPS\_B, and TPS\_old MTCMOS circuits, respectively. Similarly, high short-circuit currents are produced by the TPS\_A sleep signal modulator that is presented in [6], as discussed in Section III. The TPS\_A MTCMOS circuit consumes 11.41×5.79×, and 4.91× higher energy as compared to the single-phase, TPS\_B, and TPS\_old MTCMOS circuits, respectively, during a deactivation event. The sleep signal modulator that is utilized for the single-phase MTCMOS technique is a simple circuit that is composed of two inverters. In the SLEEP mode where the sleep transistor

TABLE III  
COMPREHENSIVE COMPARISON OF SLEEP SIGNAL SLEW RATE MODULATION TECHNIQUES

Circuit technique	Single-phase	TPS_old [10]	TPS_A [6]	TPS_B	Stepwise Vgs
Peak ground noise (mV)	2.090	2.197	1.810	1.999	2.337
TR (ns)	44.12	21.49	14.48	14.45	12.15
ER (pJ)	1.972	1.569	1.029	1.030	1.021
ED (pJ)	0.034	0.079	0.388	0.067	0.530
SLEEP leakage power (nW)	70.0	342.2	86.0	87.1	87.2
Layout area (μm <sup>2</sup> )	1505	1616	1550	1551	1573
Normalized EQM	2.10	1	7.16	9.15	7.58

is cut off (Sleep\_Local = 0 V), the single-phase MTCMOS circuit reduces the leakage power consumption by 79.54%, 19.72%, 19.63%, and 18.60% due to the simpler and smaller sleep signal modulator as compared to the TPS\_old, stepwise Vgs, TPS\_B, and TPS\_A MTCMOS circuits, respectively. Significant leakage currents are produced by the mixed-signal triple-phase sleep signal slew rate modulator (Vbias1 is gated low, while Vbias2, Vbias3, and clock are gated high in SLEEP mode). The TPS\_old MTCMOS circuit that is proposed in [9] consumes 3.93× higher leakage power as compared to the newly proposed TPS\_B MTCMOS circuit.

The single-phase MTCMOS circuit occupies the smallest silicon area. The single-phase MTCMOS circuit reduces the overall layout area by 6.87%, 4.32%, 2.97%, and 2.90% as compared with the TPS\_old, stepwise Vgs, TPS\_B, and TPS\_A MTCMOS circuits, respectively.

In order to evaluate the overall quality of different sleep signal slew rate modulated MTCMOS circuits at the typical process corner, a comprehensive electrical quality

metric (EQM) is evaluated next. The EQM is

$$EQM = (TR \times (ER + ED) \times Leakage\_Power \times Layout\_Area)$$

Where Leakage\_Power is the total leakage power consumed by a sleep signal modulator and MTCMOS circuit together in SLEEP mode (as listed in Table III). The normalized EQM (with respect to TPS\_old MTCMOS circuit) is listed in Table III. The newly proposed TPS MTCMOS circuit (TPS\_B) enhances the overall electrical quality by 9.15×, 4.35×, 1.28×, and 1.21× as compared to the old mixed-signal triple-phase [9], the single-phase, the previously proposed digital triple-phase (TPS\_A), and the stepwise Vgs MTCMOS circuits, respectively. The newly proposed TPS MTCMOS is therefore identified as the most desirable mode transition technique in ground-gated integrated circuits at the typical process corner.

**B. Influence of Process Variations**

The fluctuations of process parameters alter the electrical characteristics of CMOS circuits [21], [22]. The effects of

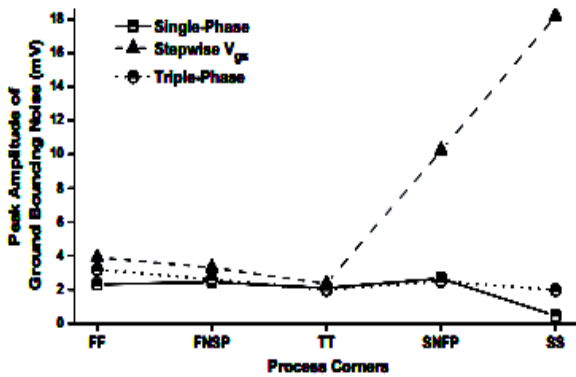


Fig. 12. Peak amplitudes of ground bouncing noise produced by sleep signal slew rate modulated MTCMOS circuits at different process corners.

Process variations on the peak ground bouncing noise, overall reactivation time, and overall reactivation energy consumption of sleep signal slew rate modulated MTCMOS circuits are evaluated in this section. The five process corners (TT: typical, FF: fast nMOS fast pMOS, FNSP: fast nMOS slow pMOS, SNFP: slow nMOS fast pMOS, and SS: slow nMOS slow pMOS) and the Monte Carlo model cards provided by the UMC 80-nm CMOS technology are used to evaluate the influence of die-to-die and within-die process variations, respectively, on MTCMOS circuits. The TPS MTCMOS circuits that are proposed in [6] and [9] are inferior to the other multiphase sleep signal slew rate modulation techniques that are evaluated in this paper even at the typical process corner. Furthermore, the additional clock signals and voltage bias sources cause significant design complexity and challenge

with the mixed-signal triple-phase sleep signal slew rate modulator that is presented in [9]. Therefore, the previously published TPS MTCMOS circuits (TPS\_old and TPS\_A) are not further evaluated in this paper.

The peak amplitudes of ground bouncing noise produced by sleep signal slew rate modulated MTCMOS circuits at different process corners are shown in Fig. 17. The strength of nMOS transistors are degraded at the SNFP and SS process corners. The parasitic capacitors attached to the internal nodes of low-|Vth| circuit block and the VGND are not discharged to sufficiently low voltage levels at the end of the relaxation period (TC in Fig. 14) With the stepwise Vgs MTCMOS circuit. When the second wake up step is initiated, therefore, significant amount of noise is produced by the stepwise Vgs MTCMOS circuit as shown in Fig. 17.

The sensitivity of reactivation noise to die-to-die process variations is characterized next. The peak noise deviations of MTCMOS circuits are evaluated. The peak noise deviation (NDEV) is given in (7), shown at the bottom of the next page, where NFF, NFNSP, NTT, NSNFP, and NSS are the peak ground bouncing noise produced by MTCMOS circuits at the FF, FNSP, typical, SNFP, and SS process corners, respectively. As listed in Table IV, the triple-phase sleep signal slew rate modulated MTCMOS circuit reduces the peak noise deviation by 92.03% and 20.22% as compared to the stepwise Vgs and single-phase sleep signal slew rate modulated MTCMOS circuits, respectively. Fully digital TPS MTCMOS circuit

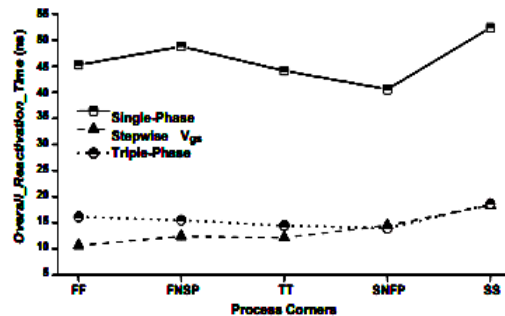


Fig.13. Overall reactivation times of sleep signal slew rate modulated MTCMOS circuits at different process corners.

Technique thereby maintains effectiveness for mode transition noise suppression across various process corners and offers the highest immunity to die-to-die process parameter fluctuations.

The overall reactivation time (TR) and overall reactivation energy (ER) of sleep signal slew rate modulated MTCMOS circuits at different process corners are shown in Figs. 18 and 19, respectively. In order to characterize the sensitivity of TR and ER of MTCMOS circuits to die-to-die process variations, the reactivation

time deviation and reactivation energy deviation of MTCMOS circuits with respect to the TR and ER at the typical process corner are evaluated. Reactivation time deviation (TR\_DEV) and reactivation energy deviation (ER\_DEV) are given in (8) and (9), shown at the bottom of the page, respectively.

As listed in Table IV, the TPS MTCMOS circuit achieves the lowest reactivation time deviation. The TPS MTCMOS circuit reduces TR\_DEV by 54.72% and 32.55% as compared to the single-phase and stepwise Vgs MTCMOS circuits, respectively. Alternatively, stepwise Vgs MTCMOS circuit displays the lowest reactivation energy deviation. Stepwise Vgs MTCMOS circuit reduces ER\_DEV by 82.91% and 37.21% as compared to the single-phase and triple-phase MTCMOS circuits, respectively. Next, the MTCMOS sleep signal slew rate modulation techniques are compared under within-die process variations. 1000 Monte Carlo simulations are run to evaluate the statistics for peak ground bouncing noise, overall reactivation time, and overall reactivation energy consumption of different MTCMOS circuits. The Monte Carlo SPICE model cards provided by UMC are used for the simulations. The UMC 80-nm CMOS technology Monte Carlo SPICE model cards are based on real wafer measurements [23]. Threshold voltage,

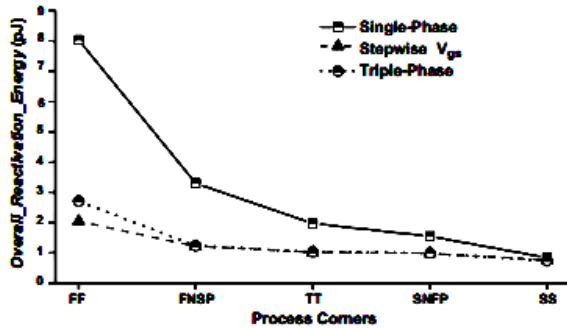


Fig.14. Overall reactivation energy consumptions of sleep signal slew rate modulated MTCMOS circuits at different process corners.

Table IV

Comprehensive Comparison MTCMOS Circuit Techniques under Process Variations

Circuit technique	Single-phase	Triple-phase	Stepwise V <sub>gs</sub>
N <sub>DEV</sub> (mV)	0.89	0.71	8.91
TR_DEV (ns)	5.08	2.30	3.41
ER_DEV (pJ)	3.16	0.86	0.54
N <sub>SD</sub> (mV)	0.81	0.32	1.36
TR_SD (ns)	1.77	0.90	0.91
ER_SD (pJ)	0.47	0.13	0.14
Normalized PIARM	1	183.10	3.39

gate oxide thickness, carrier mobility, and channel doping concentration related parameters are assumed to have Gaussian distributions in the Monte Carlo SPICE model cards. The statistics for the peak ground bouncing noise, overall reactivation time, and overall reactivation energy consumption of MTCMOS circuits are illustrated in Figs. 20-22, respectively. The standard deviations of peak ground bouncing noise (N<sub>SD</sub>), overall reactivation time (T<sub>R\_SD</sub>), and overall reactivation energy consumption (E<sub>R\_SD</sub>) are listed in Table IV.

The proposed digital triple-phase sleep signal slew rate modulator has the capability to initiate different phases of a reactivation process by monitoring the voltage levels of Sleep\_Local and VGND. Triple-phase MTCMOS circuit thereby displays the smallest standard deviations of peak ground bouncing noise, overall reactivation time, and overall reactivation energy consumption under within-die process variations as listed in Table IV. Triple-phase MTCMOS circuit reduces the standard deviations of peak ground bouncing noise, overall reactivation time, and overall reactivation energy consumption by up to 76.47%, 49.15%, and 72.34%, respectively, as compared to the other MTCMOS circuits

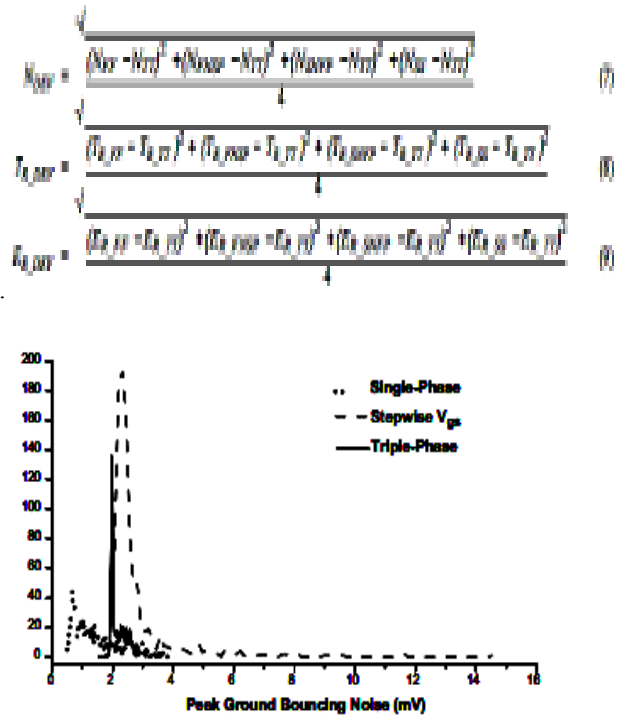


Fig.15. Statistical distribution of peak ground bouncing noise with different MTCMOS circuit techniques under within-die process variations.

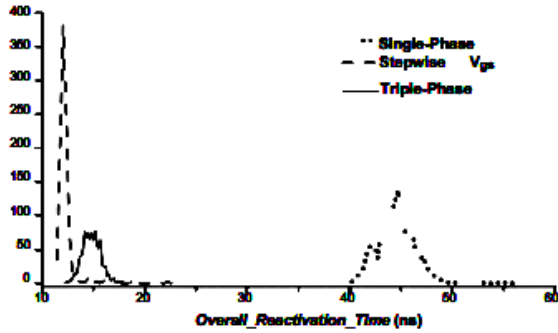


Fig.16 Statistical distribution of overall reactivation time with different MTCMOS circuit techniques under within-die process variations

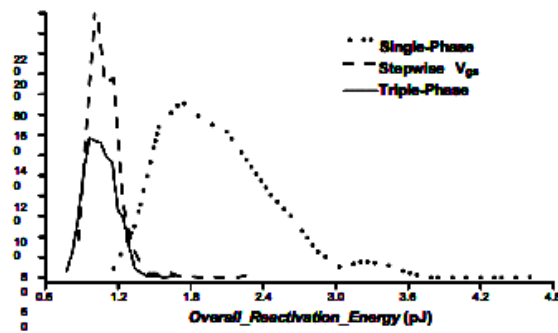


Fig.17. Statistical distribution of overall with different MTCMOS circuit techniques under within-die process variations

In order to evaluate the overall performance of sleep signal slew rate modulated MTCMOS circuits under die-to-die and within-die process parameter variations, a comprehensive *process imperfections aware robustness metric (PIARM)* is evaluated next. *PIARM* is

$$PIARM = \frac{1}{N_{DEV} \times T_{R\_DEV} \times E_{R\_DEV} \times N_{SD} \times T_{R\_SD} \times E_{R\_SD}} \quad (10)$$

The normalized *PIARM* (with respect to single-phase MTCMOS circuit) is listed in Table IV. The TPS MTCMOS circuit enhances the *PIARM* by 183.1× and 54.06× as compared to the single-phase and stepwise  $V_{gs}$  sleep signal slew rate modulated MTCMOS circuits, respectively. Digital TPS is identified as the most robust technique for achieving fast and energy efficient mode transitions with negligible reactivation noise in MTCMOS circuits under process parameter fluctuations.

**VI. Conclusion**

Sleep signal slew rate modulation techniques are explored in this paper for reducing mode transition noise in

MTCMOS circuits. A triple-phase sleep signal slew rate modulation technique with a novel digital sleep signal generator is proposed. The new digital TPS technique enhances the overall electrical quality by 9.15×4.35× and 1.21× as compared to previously published mixed-signal triple-phase, single-phase, and step wise  $V_{gs}$  sleep signal slew rate modulated MTCMOS circuits, respectively, under an equal-noise constraint at the typical process corner in a UMC 80-nm CMOS technology. Furthermore, the digital TPS technique is identified as the most robust MTCMOS circuit technique among the MTCMOS circuits that are evaluated in this paper under both die-to die and within-die process parameter variations. The triple phase sleep signal slew rate modulation technique enhances the overall tolerance to process parameter fluctuations by up to 183.1× and 54.06× as compared to the single-phase and stepwise  $V_{gs}$  sleep signal slew rate modulation techniques, respectively, based on a comprehensive robustness metric.

**References**

- [1] B.H.Calhoun, F.A. Honoré, and A. P. Chandrakasan, "A leakage reduction methodology for distributed MTCMOS," IEEE J. Solid-State Circuits, vol. 39, no. 5, pp. 818–826, May 2004.
- [2] H. Jiao and V.Kursun, "Sleep signal slew rate modulation for mode transition noise suppression in ground gated integrated circuits," in Proc. IEEE Int. SoC Conf., Sep. 2011, pp. 365–370.
- [3] H. Jiao and V.Kursun, "Ground-bouncing-noise-aware combinational MTCMOS circuits," IEEE Trans. Circuits Syst. I, Reg. Papers, vol. 57, no. 8, pp. 2053–2065, Aug. 2010.
- [4] H. Jiao and V.Kursun, "Ground bouncing noise suppression techniques for data preserving sequential MTCMOS circuits," IEEE Trans. Very Large Scale Integr. (VLSI) Syst., vol. 19, no. 5, pp. 763–773, May 2011.
- [5] H. Jiao and V. Kursun, "Threshold voltage tuning for faster activation with lower noise in tri-mode MTCMOS circuits," IEEE Trans.
- [6] S. Henzler, M. Eireiner, J. Berthold, G. Georgakos, and D.SchmittLandsiedel, "Activation technique for sleep-transistor circuits for reduced power supply noise," in Proc. IEEE Eur.
- [7] S. Kim, S. V. Kosonocky, D. R. Knebel, K. Stawiasz, D. Heidel, and M. Immediato, "Minimizing inductive noise in system-on-a-chip with multiple power gating structures," in Proc.
- [8] S. Paik, S. Kim, and Y. Shin, "Wakeup synthesis and its buffered tree construction for power gating circuit designs," in Proc. IEEE/ACM Int. Symp. Low Power Electron. Design, Aug. 2010, pp. 413–418

- [9] H. Jiao and V. Kursun, "Noise-aware data preserving sequential MTCMOS circuits with dynamic forward body bias," *J. Circuits, Syst., Comput.*, vol. 20, no. 1, pp. 125–145, Feb. 2011.